Degradation of Fibrillar Collagen in a Human Melanoma Xenograft Improves the Efficacy of an Oncolytic Herpes Simplex Virus Vector

Trevor D. McKee,[1,2] Paola Grandi,[5] Wilson Mok,[1,3] George Alexandrakis,[1] Numpon Insin,[4] John P. Zimmer,[4] Moungi G. Bawendi,[4] Yves Boucher,[1] Xandra O. Breakefield,[5] and Rakesh K. Jain[1]

[1]Edwin L. Steele Laboratory, Department of Radiation Oncology, Massachusetts General Hospital, Harvard Medical School, Boston, Massachussetts; [2]Biological Engineering Division, [3]Departments of Chemical Engineering and [4]Chemistry, Massachusetts Institute of Technology, Cambridge, Massachussetts; and [5]Departments of Neurology and Radiology, Massachusetts General Hospital, and Neuroscience Program, Harvard Medical School, Charlestown, Massachussetts

Abstract

Oncolytic viral therapy provides a promising approach to treat certain human malignancies. These vectors improve on replication-deficient vectors by increasing the viral load within tumors through preferential viral replication within tumor cells. However, the inability to efficiently propagate throughout the entire tumor and infect cells distant from the injection site has limited the capacity of oncolytic viruses to achieve consistent therapeutic responses. Here we show that the spread of the oncolytic herpes simplex virus (HSV) vector MGH2 within the human melanoma Mu89 is limited by the fibrillar collagen in the extracellular matrix. This limitation seems to be size specific as nanoparticles of equivalent size to the virus distribute within tumors to the same extent whereas smaller particles distribute more widely. Due to limited viral penetration, tumor cells in inaccessible regions continue to grow, remaining out of the range of viral infection, and tumor eradication cannot be achieved. Matrix modification with bacterial collagenase coinjection results in a significant improvement in the initial range of viral distribution within the tumor. This results in an extended range of infected tumor cells and improved virus propagation, ultimately leading to enhanced therapeutic outcome. Thus, fibrillar collagen can be a formidable barrier to viral distribution and matrix-modifying treatments can significantly enhance the therapeutic response. (Cancer Res 2006; 66(5): 2509-13)

Introduction

Oncolytic vectors, mutant viruses that replicate preferentially in tumor cells, have shown promise in various preclinical tumor models (1). Oncolytic viral therapy employs a novel method of tumor destruction mediated by viral replication and selective lysis of cancer cells (2). Creation of more virus by infected tumor cells and the resultant infectious spread improve performance over more passive forms of therapeutic delivery (3, 4). Early-phase human trials of G207, an oncolytic herpes simplex virus (HSV) vector, for treatment of recurrent malignant glioblastomas have shown both safety and efficacy (5). However, the inability to efficiently propagate and infect cells distant from the injection site limits the capacity of oncolytic viruses to achieve consistent therapeutic responses (6). In this study, we show that fibrillar collagen, a major barrier to macromolecular transport in the tumor interstitium (7–9), also limits HSV vector distribution within a melanoma. Direct degradation of the fibrillar collagen network improves viral distribution, leading to improved oncolytic viral therapy.

Materials and Methods

Viral vectors. The HSV-1 recombinant viruses used in this study were the replication defective mutant Gal4 (*ICP4*$^-$, *lacZ*$^+$; from Dr. Neal DeLuca, University of Pittsburgh, Pittsburgh, PA; ref. 10) and MGH2 (*ICP6*$^-$, *γ34.5*$^-$, *eGFP*$^+$; from Drs. E. Antonio Chiocca and Yoshi Saeki, The Ohio State University, Columbus, OH). MGH2 is a replication conditional virus attenuated by two nonessential viral gene deletions, *ICP6* and *γ34.5* (11). Virus replication is impaired in nondividing cells but not in tumor cells.

Gal4 and MGH2 stocks were propagated in E5 and E26 cells (from Dr. Neal DeLuca; ref. 12), respectively, which supply the HSV-1 ICP4 protein (E5) or HSV ICP4 and ICP27 proteins (E26) *in trans*. To obtain GFP-labeled HSV particles, E5 and E26 cells were transfected with a plasmid encoding the fusion protein VP16-GFP (pVP16-GFP; ref. 13) and infected with Gal4 and MGH2, respectively. After purification and concentration, the titer of each virus preparation was quantified by counting *lacZ*-positive cells for Gal4 and GFP-positive cells for MGH2.

Dorsal skinfold window preparation. Human melanoma Mu89 cells were grown in dorsal skinfold chambers in severe combined immunodeficient (SCID) mice as previously described (9). All animal experiments were done with the approval of the Institutional Animal Care and Use Committee.

Injection and imaging of labeled vectors and tracers. For dorsal chamber tumor studies, HSV vectors labeled with VP16-GFP were mixed with either 0.2 μg/μL bacterial collagenase (Sigma, C0773, St Louis, MO) or PBS to a final titer of 10^6 transducing units/μL. For microsphere experiments, quantum dot–encoded silica microspheres were synthesized according to a previously developed procedure (14). For all injections, 1 μL of solution was infused into the tumor at constant pressure (~1 μL/10 minutes) using a glass micropipette connected to a syringe pump. Images were obtained using a custom-built multiphoton laser scanning microscope (9) using a 20× 0.5 numerical aperture objective lens. Excitation was at 880 nm, with simultaneous detection of second harmonic generation (9) via a 435DF30 emission filter and GFP via a high-pass 475 dichroic and a 525DF100 emission filter. Cascade blue–conjugated dextran was visualized by exciting at 780 nm and imaging the same region (for Cascade blue–conjugated dextran and GFP), followed by image registration. Microspheres (containing 642-nm maximum emission quantum dots) were imaged with a 610DF70 emission filter. Three-dimensional image stacks containing 20 images of 5-μm thickness were obtained wherever fluorescence intensity

Note: Supplementary data for this article are available at Cancer Research Online (http://cancerres.aacrjournals.org/).

T.D. McKee, P. Grandi, and W. Mok contributed equally to this work.

Requests for reprints: Rakesh K. Jain, Edwin L. Steele Laboratory, Department of Radiation Oncology, Massachusetts General Hospital, 100 Blossom Street, Cox 7, Boston, MA 02114. Phone: 617-726-4083; Fax: 617-724-1819; E-mail: jain@steele.mgh.harvard.edu.

doi:10.1158/0008-5472.CAN-05-2242

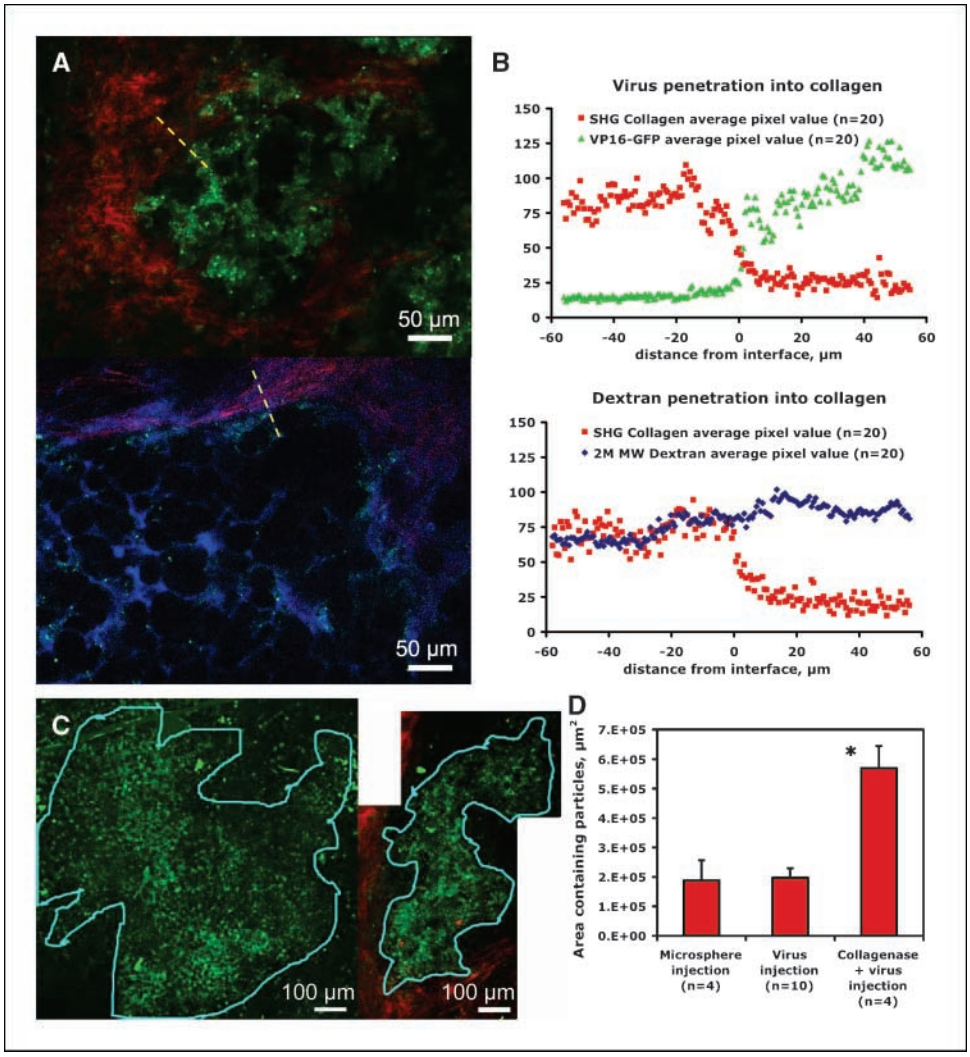

Figure 1. Viral vector distribution following intratumoral injection. *A,* multiphoton images of Mu89 melanomas 30 minutes after intratumoral injection of VP16-GFP labeled Gal4 vectors (*green*), either alone (*top*) or with Cascade blue–conjugated dextran (*blue; bottom*). Second-harmonic generation signal denotes fibrillar collagen (*red pseudocolor*). HSV vectors localized in extracellular spaces around individual tumor cells and were excluded by areas of intense second-harmonic generation signal. In contrast, the smaller dextran tracer penetrated regions rich in fibrillar collagen. *B,* relative localization of collagen and injected particles determined by pixel analysis. Spatial comparison of pixel intensities was done for collagen (*red pixels*) and either viral particles (*green pixels; top*) or dextran (*blue pixels; bottom*). Analysis was done along lines drawn perpendicular to the border of second-harmonic generation signal and mean values were plotted. A representative image and line are shown for each case (*A, yellow lines*). Collagen and viral localization in the tumor are inversely correlated. *C,* multiphoton images of viral vector distribution following coinjection with collagenase (*left*) compared with injection of virus alone (*right*). Each image is a montage of several multiphoton images. This area of distribution is outlined in blue in each case. *D,* comparison of the area of viral vector and microsphere distribution following intratumoral injection. Areas measured from a maximum intensity projection of 10 images taken ~30 minutes following injection. Collagenase and virus coinjection resulted in a nearly 3-fold increase in the area of viral distribution compared with microspheres and HSV particles alone ($P < 0.05$).

from the injected particles was detected. A maximum intensity z-projection of each colored stack generated a two-dimensional image. Images of consecutive adjacent regions in the x and y directions were combined into a montage, generating a single image of the entire injection site.

Image analysis. The pixel intensities of collagen (red pixels) and injected particles (viral vectors, green pixels; dextran, blue pixels) were spatially compared along lines drawn perpendicular to the periphery of virus containing regions. Analysis was done for one injection in each case, in five distinct image stacks, and at different depths, for a total of 20 lines measured within each tumor. The mean pixel intensities were plotted as a function of the relative distance from the observed interface with fibrillar collagen. All lines were registered such that the largest change in second-harmonic generation intensity was maintained at the origin of the graph.

For quantification of viral vector distribution following injection, the entire area of viral distribution was outlined on the images. The border of the viral focus was determined as the location at which the intensity dropped to 10% of the mean intensity at the center of injection. The calculation of the area was done with imaging software (ImageJ, U.S. NIH, Bethesda, MD).[6]

Flank tumor growth delay. Mu89 cells were implanted s.c. in the flank of SCID mice and allowed to reach 100 mm^3 average volume. Mice were then randomized into four groups (six to seven animals per group) and given 10 μL intratumoral injections of either PBS, 1.0 μg collagenase, 10^6 transducing units of MGH2, or a mixture of 10^6 transducing units of MGH2 and 1.0 μg collagenase. A second injection was done 2 days later. Tumor volume was measured every 2 to 3 days and calculated as volume = πAB^2 / 6, where A and B are maximum and minimum diameters, respectively. Mice died from natural progression of disease or were euthanized when (*a*) tumor mass exceeded a size of 2,000 mm^3 or (*b*) premorbid behavior was noted. For tumors failing to reach 10 times the initial volume due to morbidity, the time to last measurement substituted as a conservative approximation of growth.

Statistical analysis. Data are expressed as mean ± SE. Statistical significance between groups was determined by unpaired Student's t test. Statistical analysis was done with the StatView 4.51 software (SAS Institute, Inc., Cary, NC). Differences were considered statistically significant at $P < 0.05$.

Results

Distribution of virion particles is hindered by collagen-rich regions. To quantify virus distribution, 1 μL containing 10^6 viral transducing units of VP16-GFP labeled nonreplicative HSV-1 virions (Gal4) was directly injected into Mu89 human melanomas grown in dorsal skin windows in SCID mice. *In vivo*, multiphoton imaging of viral particles with simultaneous second-harmonic generation imaging of fibrillar collagen was done ~30 minutes following injection. Viral particles distributed primarily within collagen-free areas of the tumor with limited penetration into

[6] http://rsb.info.nih.gov/ij/.

collagen-rich regions (Fig. 1*A*). To quantify viral penetration, pixel counts of collagen (second-harmonic generation) and virus (GFP) were measured along lines perpendicular to the periphery of virus containing regions (one example line is shown in Fig. 1*A*). Averaging over 20 lines per injection revealed an inverse correlation between collagen and viral particles, such that an increase in the amount of fibrillar collagen present corresponded to a sharp decrease in virus signal (Fig. 1*B*). Whereas collagen is known to hinder macromolecular transport (7, 8), nearly complete exclusion to this extent has not been seen. To directly compare viral distribution with another macromolecular tracer, Cascade blue–conjugated 2×10^6 molecular weight dextran tracer molecules ($R_H \sim 20$ nm) were coinjected with HSV vectors. Whereas the dextran penetrated into collagen-rich regions, viral particles were excluded (Fig. 1*A* and *B*). In the collagen-containing regions, the mean dextran intensity is significantly greater than the mean virus intensity when both are normalized to the maximum signal from each channel ($P < 0.001$). To further clarify the role of particle size in collagen exclusion, quantum dot–loaded microspheres similar in size to HSV particles (~ 150 nm diameter) were directly injected into Mu89 tumors. As with HSV particles, these microspheres were excluded from collagen-rich tumor areas (Supplementary Fig. S2). The microsphere distribution areas were similar to those of HSV vectors (Fig. 1*D*).

Disruption of the collagen network results in improved virus distribution and gene expression. To test whether disruption of collagen could improve viral penetration into tumors, viral vectors were coinjected with bacterial collagenase (0.2 μg/μL). Collagenase increased the area of viral distribution by nearly 3-fold compared with control injections (Fig. 1*D*). Rather than distributing into restricted regions bounded by fibrillar collagen, vectors spread more uniformly from the injection site with collagenase treatment (Fig. 1*C*).

Collagenase enhances the efficacy of oncolytic viral therapy. The oncolytic virus MGH2 has the same backbone as G207 (11) but carries the *GFP* reporter gene instead of *lacZ*. MGH2 replicates in Mu89 melanoma cells in culture, resulting in GFP expression and cell lysis within 24 to 48 hours (data not shown). MGH2 (10^6 transducing units) was injected into Mu89 tumors as before (Fig. 2). Initial viral distribution was again limited by fibrillar collagen (data not shown). The area of infection was subsequently localized to only a small proportion ($\sim 15\%$) of the entire tumor mass, corresponding to the site of injection (Fig. 2*A, middle*). Even 11 days following the initial injection of MGH2, viral vectors could not penetrate sufficiently to infect the entire tumor mass (Fig. 2*A, bottom*). No significant treatment response was observed in any of the tumors injected with MGH2 alone or with bacterial collagenase alone (Fig. 2*A* and *C, bottom*).

In contrast, when the same amount of oncolytic virus was coinjected with collagenase (0.2 μg/μL), the initial viral distribution was greater relative to virus alone (data not shown), translating into an improved area of tumor cell infection (Fig. 2*B, middle*). Therapeutic response was observed in all four collagenase cotreated tumors with a significant decrease in tumor size in two cases (Fig. 2*B, bottom*).

We then tested if the coinjection of collagenase and MGH2 would increase the therapeutic efficacy of MGH2 over longer time intervals. When Mu89 tumors growing in the flank of SCID mice reached 100 mm^3, they were injected intratumorally with either 1 μg collagenase, 10^6 transducing units of MGH2, or both collagenase and MGH2, followed by similar injections 2 days later. Control tumors were injected with PBS alone. The time for the tumor to reach 10 times the initial volume (mean ± SE) was compared for each group (Fig. 3). Both collagenase treatment alone (19 ± 1 days) and MGH2 injection alone (27 ± 3 days) had no significant effect on tumor growth compared with PBS control (24 ± 3 days; $P > 0.05$, both cases). With MGH2 treatment alone, one tumor showed marked regression but recurred after 10 days. Coinjection of MGH2 with collagenase (50 ± 8 days) significantly delayed the growth of tumors compared with all other treatment groups ($P < 0.05$ for all

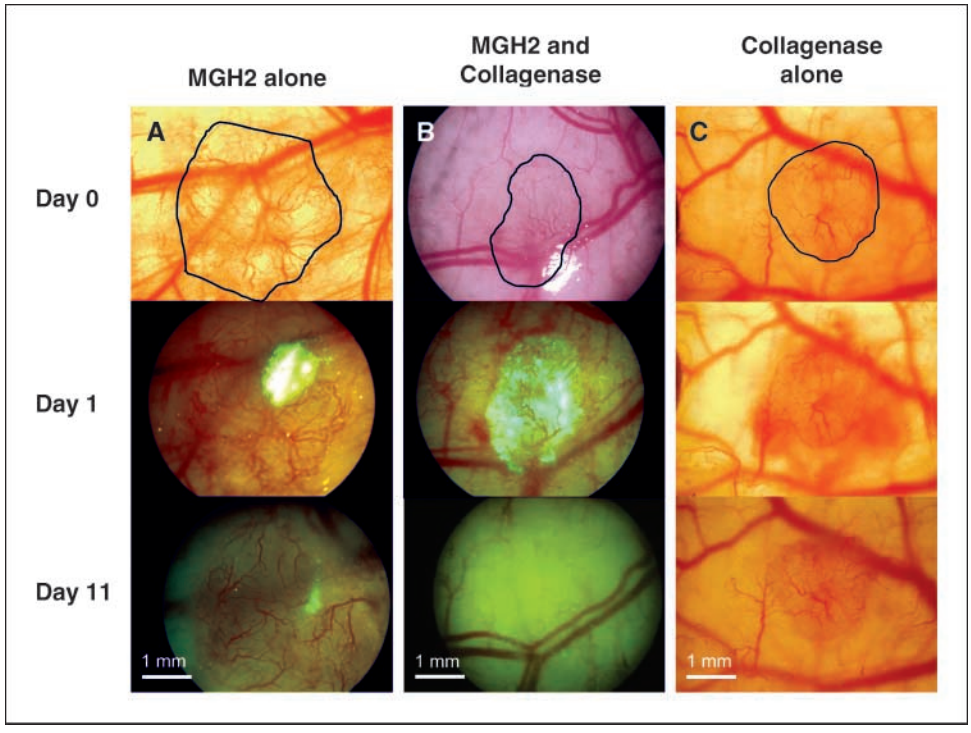

Figure 2. Effect of collagenase on oncolytic viral therapy. Mu89 melanomas implanted in the dorsal skinfold chamber of SCID mice were treated with the oncolytic vector MGH2 in combination with PBS (*A*) or MGH2 in combination with collagenase (*B*). Collagenase treatment alone is shown in (*C*) for comparison. $N = 4$ for all three treatment groups. Representative bright-field images of tumors before injection (tumors outlined in black, *top*). Representative fluorescent microscopic images of tumors 1 day (*middle*) and 11 days (*bottom*) after injection. Infection of tumor cells was detected by expression of the reporter gene GFP (encoded by the virus). Coinjection of MGH2 and collagenase resulted in a greater distribution of infected cells (*B, middle*) relative to injection of MGH2 alone (*A, middle*). At 11 days, regression of the tumor (as evidenced by absence of tumor vasculature) was achieved with MGH2 and collagenase coinjection (*B, bottom*) whereas no significant change in volume was observed with MGH2 treatment alone (*A, bottom*). Collagenase-treated tumors recover from any induced hemorrhage by day 11 (*C, bottom*).

cases). Two of seven tumors failed to grow to 200 mm^3, even 60 days after treatment; a third experienced apparently complete regression although it recurred 20 days later.

Improved efficacy is due to initial improved distribution of viral particles. To investigate the mechanism of improved efficacy, tumors were treated as before with MGH2, either alone or with collagenase, and analyzed 2 days after the second injection. Tissue sections were stained for structural virion proteins, counterstained for nuclei (4′,6-diamidino-2-phenylindole), and imaged for GFP expression using confocal microscopy to determine viral distribution. As expected, HSV antigen was present within and surrounding cells expressing GFP. In MGH2-treated tumors, virion particles and infected cells distributed in a localized fashion reminiscient of the needle track (Supplementary Fig. S1*A*). In contrast, for MGH2 and collagenase treatment, a diffuse distribution of infected cells was observed throughout the entire tumor section, spanning an area of up to 3 × 7 mm (Supplementary Fig. S1*B*). Later time points showed continued viral spread but only within collagen-free areas.

Discussion

The development of strategies to improve both the initial vector distribution within tumors and the ability of these vectors to propagate through the entire tumor mass is critical to the success of oncolytic viral therapy (1). Previous reports show that protease pretreatment can increase the therapeutic efficacy of a nonreplicative viral vector (15). However, the mechanism of improved efficacy was undefined due to the use of nonspecific digestive enzymes, normally used to dissociate tissues, which degrade multiple extracellular matrix components. Thus, we wished to determine whether fibrillar collagen, previously shown to be a major barrier to macromolecular diffusion in tumors (7, 8), is the matrix component which limits viral distribution in certain tumors.

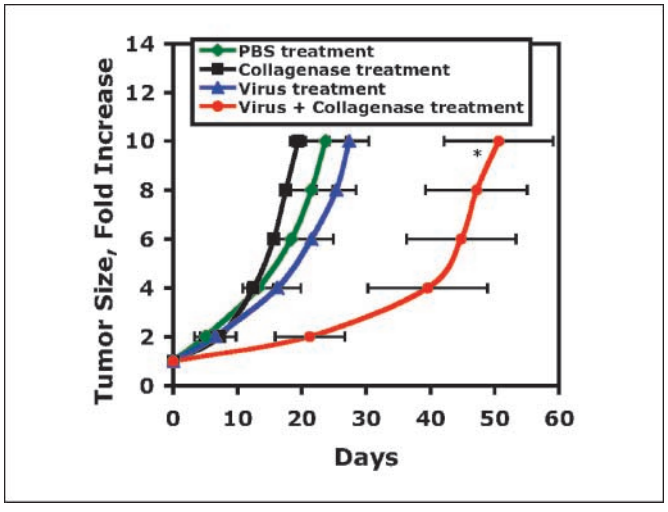

Figure 3. Effect of collagenase on MGH2-induced tumor growth delay. Tumors were grown s.c. in the hind flank of SCID mice. When tumors reached ~100 mm^3, animals were divided into four groups (n = 6-7) and treated twice (day 0 and day 2) with 10 μL of PBS (*green*), collagenase (0.1 μg/μL; *black*), MGH2 (10^6 transducing units) in PBS (*blue*), or MGH2 (10^6 transducing units) and collagenase (0.1 μg/μL) in PBS (*red*). Tumor volumes were measured every 2 to 3 days. *Points,* mean time to reach a given volume for each group; *bars,* SE. The time to reach 10 times the initial volume was compared. There was no significant difference between PBS (24 ± 3 days) and either collagenase treatment alone (19 ± 1 days) or MGH2 alone (27 ± 3 days; $P > 0.05$ for both cases). However, MGH2 and collagenase cotreatment (50 ± 8 days) induced a significant tumor growth delay relative to all other groups ($P < 0.05$ for all cases).

Our results show the important role that fibrillar collagen can play in regulating the initial distribution of viral vectors in certain fibrous tumors. Whereas smaller tracers (2×10^6 MW dextran, R_H ~20 nm, as well as immunoglobulin G, R_H ~5 nm; data not shown) distributed relatively uniformly within the tumor, the vast majority of HSV virions (150 nm in diameter) were located only in collagen-poor areas. Furthermore, silica microspheres similar in size to the viral particles, but lacking their ability to bind to cell and matrix proteins, were excluded from collagen (Supplementary Fig. S2). This suggests that the effective pore size cutoff of the collagen network is smaller than the size of these viral particles. This may have a significant effect because many tumors in humans show extensive stromal infiltration with extracellular matrix and collagen deposition (16).

Fibrillar collagen is also important in the propagation of oncolytic viral vectors through the tumor. Oncolytic vectors are thought to overcome some of the delivery issues faced by nonreplicating viral vectors through their ability to propagate on site in tumors (thereby amplifying the input dose) and spread from tumor cell to tumor cell. We found that the collagen network, in addition to restricting the initial distribution, limited the maximal spread of MGH2 infection within the tumor. Tumor cell infection remained confined to a small area and the tumor continued to grow. Coinjection of MGH2 with collagenase resulted in a broad, uniform distribution of viral particles and infected cells, with substantial tumor regression and enhanced efficacy. This dispersed distribution of virus can improve therapeutic outcome in several ways: (*a*) the broad initial virion distribution improves the chance that viral vectors can penetrate all regions of the tumor; (*b*) the occurrence of multiple infections of the same tumor cell decreases whereas the number of distinct tumor cell infections increases; and (*c*) once the virus replicates and lyses the cell it has infected, it has access to a greater number of previously uninfected neighboring cells. All together, these processes can lead to increased oncolytic activity as shown schematically in Fig. 4.

Researchers have developed other methods to try to overcome the limited distribution of oncolytic vectors in tumors (17). Some use multiple injections, either on successive days or with fractionation of the initial dose at multiple sites (18). However, in the absence of extracellular matrix modification, viral distribution at each individual injection site would still be limited by collagen. Indeed, a phase II trial with an oncolytic adenoviral vector showed limited improvement in efficacy even with daily injections that included fractionation (19).

We noted that intratumoral hemorrhages occurred in many tumors treated with collagenase. Whereas bleeding from collagenase treatment alone did not affect tumor growth, this phenomenon shows the complex interactions between the extracellular matrix and cells within the tumor, including both tumor and host endothelial cells. It is possible that collagenase treatment of tumors may increase the risk of metastasis although no increase in metastasis was observed in our preliminary study (Supplementary Table S1) or a previous study in which tumors were treated with direct injections of proteases (collagenase/dispase, trypsin; ref. 15). The development of this matrix-modulating technique for clinical applications may require the use of specific matrix proteases, such as matrix metalloproteinase 8, which degrades collagen and has been shown to decrease metastasis (20).

In conclusion, we determined that even with the on-site generation of viral particles provided by the replication-competent nature of an oncolytic HSV vector, fibrillar collagen still prevents viral spread throughout the tumor in a melanoma model. Collagen

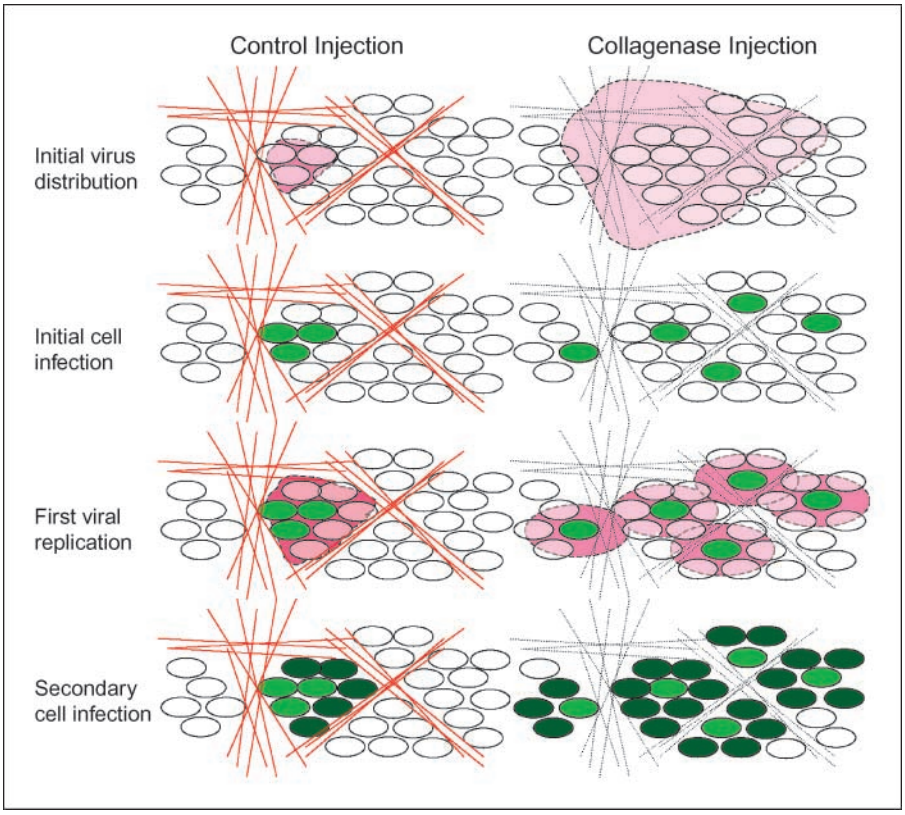

Figure 4. A representative model of improvement in oncolytic viral distribution and tumor cell infection by collagenase treatment. Following direct intratumor injection, viral spread (*red area*) is limited by fibrillar collagen (*red lines*) and results in a cluster of infected cells (*light green*). The collagen network also restricts the distribution of subsequent viral progeny and tumor cell infection beyond the initial injection site is not achieved. In contrast, coinjection of virus with collagenase results in a more diffuse distribution of viral particles and a greater number of initially infected cells (*light green*). Viral particles released by these cells have greater access to neighboring uninfected cells. This process results in more widespread secondary infection (*dark green*) and ultimately greater therapeutic efficacy.

network disruption increases initial vector distribution and subsequent propagation through the tumor mass, significantly improving therapeutic outcome. This result has implications for other viral particles, gene delivery strategies, and nanotechnology-based delivery systems, as all face the problem of insufficient delivery to the target cells. Furthermore, any method decreasing tumor collagen content may have similar effects. These findings suggest ways to increase the potency of gene therapy in certain types of cancer and other diseases.

Acknowledgments

Received 6/27/2005; revised 12/12/2005; accepted 1/17/2006.

Grant support: Program Project Grant (PO1CA80124) from the National Cancer Institute to R.K. Jain and Y. Boucher.

The costs of publication of this article were defrayed in part by the payment of page charges. This article must therefore be hereby marked *advertisement* in accordance with 18 U.S.C. Section 1734 solely to indicate this fact.

We thank Sylvie Roberge and Carolyn Smith for excellent technical assistance, Sergey Kozin and Peigen Huang for assistance with mouse experiments, E. Antonio Chiocca and Yoshi Saeki for providing MGH2, Juliet Fernandez for help with vector preparations, and Mike Booth for helpful discussions.

References

1. Everts B, van der Poel HG. Replication-selective oncolytic viruses in the treatment of cancer. Cancer Gene Ther 2005;12:141–61.
2. Chiocca EA. Oncolytic viruses. Nat Rev Cancer 2002;2:938–50.
3. Ichikawa T, Chiocca EA. Comparative analyses of transgene delivery and expression in tumors inoculated with a replication-conditional or -defective viral vector. Cancer Res 2001;61:5336–9.
4. Lee CT, Park KH, Yanagisawa K, et al. Combination therapy with conditionally replicating adenovirus and replication defective adenovirus. Cancer Res 2004;64:6660–5.
5. Markert JM, Medlock MD, Rabkin SD, et al. Conditionally replicating herpes simplex virus mutant, G207 for the treatment of malignant glioma: results of a phase I trial. Gene Ther 2000;7:867–74.
6. Harrison D, Sauthoff H, Heitner S, Jagirdar J, Rom WN, Hay JG. Wild-type adenovirus decreases tumor xenograft growth, but despite viral persistence complete tumor responses are rarely achieved-deletion of the viral E1b-19-kD gene increases the viral oncolytic effect. Hum Gene Ther 2001;12:1323–32.
7. Netti PA, Berk DA, Swartz MA, Grodzinsky AJ, Jain RK. Role of extracellular matrix assembly in interstitial transport in solid tumors. Cancer Res 2000;60:2497–503.
8. Pluen A, Boucher Y, Ramanujan S, et al. Role of tumor-host interactions in interstitial diffusion of macromolecules: cranial vs. subcutaneous tumors. Proc Natl Acad Sci U S A 2001;98:4628–33.
9. Brown E, McKee T, diTomaso E, et al. Dynamic imaging of collagen and its modulation in tumors *in vivo* using second-harmonic generation. Nat Med 2003;9:796–800.
10. Chiocca EA, Choi BB, Cai WZ, et al. Transfer and expression of the lacZ gene in rat brain neurons mediated by herpes simplex virus mutants. New Biol 1990;2:739–46.
11. Kramm CM, Chase M, Herrlinger U, et al. Therapeutic efficiency and safety of a second-generation replication-conditional HSV1 vector for brain tumor gene therapy. Hum Gene Ther 1997;8:2057–68.
12. Samaniego LA, Webb AL, DeLuca NA. Functional interactions between herpes simplex virus immediate-early proteins during infection: gene expression as a consequence of ICP27 and different domains of ICP4. J Virol 1995;69:5705–15.
13. Bearer EL, Breakefield XO, Schuback D, Reese TS, LaVail JH. Retrograde axonal transport of herpes simplex virus: evidence for a single mechanism and a role for tegument. Proc Natl Acad Sci U S A 2000;97:8146–50.
14. Chan Y, Zimmer JP, Stroh M, et al. Incorporation of luminescent nanocrystals into monodisperse core-shell silica microspheres. Adv Mater (FRG) 2004;16:2092–7.
15. Kuriyama N, Kuriyama H, Julin CM, Lamborn KR, Israel MA. Protease pretreatment increases the efficacy of adenovirus-mediated gene therapy for the treatment of an experimental glioblastoma model. Cancer Res 2001;61:1805–9.
16. Elenbaas B, Weinberg RA. Heterotypic signaling between epithelial tumor cells and fibroblasts in carcinoma formation. Exp Cell Res 2001;264:169–84.
17. Jia W, Zhou Q. Viral vectors for cancer gene therapy: viral dissemination and tumor targeting. Curr Gene Ther 2005;5:133–42.
18. Currier MA, Adams LC, Mahller YY, Cripe TP. Widespread intratumoral virus distribution with fractionated injection enables local control of large human rhabdomyosarcoma xenografts by oncolytic herpes simplex viruses. Curr Gene Ther 2005;12:407–16.
19. Nemunaitis J, Khuri F, Ganly I, et al. Phase II trial of intratumoral administration of ONYX-015, a replication-selective adenovirus, in patients with refractory head and neck cancer. J Clin Oncol 2001;19:289–98.
20. Montel V, Kleeman J, Agarwal D, Spinella D, Kawai K, Tarin D. Altered metastatic behavior of human breast cancer cells after experimental manipulation of matrix metalloproteinase 8 gene expression. Cancer Res 2004;64:1687–94.